Oxidation features of sintered SiC composites deposited on E110 alloy at 1200 ^{0}C in air for fuel cladding studies

B K Afornu, A M Lider, E B Kashkarov and M S Syrtanov
Tomsk Polytechnic University, Russia, Tomsk, Lenin Ave., 30, 634050

E-mail: afornu@tpu.ru

Abstract. Protective coatings are designed to reduce oxidation under extreme reactor temperature conditions. This study involves the application of a SiC coating on an E110 (Zr-1Nb) substrate in an atmosphere of air and argon by selective laser sintering (SLS) technique in which high-temperature oxidation test (HT-Ox) was performed on samples at a temperature of 1200 ^{0}C in air for 600 seconds. Calculated mass gained after HT-Ox test gave 34.6 mg/ cm^2, 31.1 mg/cm^2, and 22.8 mg/cm^2 for uncoated E110 alloy, SiC-E110 sintered in air and SiC-E110 sintered in an argon atmosphere respectively. X-ray diffraction (XRD) phase studies show the formation of more than 90% ZrO2 on the uncoated E110 alloy after HT-Ox. SiO2 and YAlO3 accounted for more than 50% of the oxides formed on the surfaces of samples coated with SiC after a HT-Ox test. Higher coating hardness's with lower indentation depths were consistently observed in the SiC coated specimen before and after HT-Ox tests proving stability in the coated samples while higher indentation depths and sudden quadrupling in hardness was recorded in E110 alloy before and after HT-Ox respectively. SiC coating on Zr-alloy plays a significant role in reducing oxidation, especially in coatings fabricated in an inert environment.

1. Introduction

Selective Laser Sintering (SLS) is an Additive manufacturing (AM) 3D printing technology, which is rapidly gaining applications in various fields [1]. This application comprises ceramics for fuels as well as structural components of nuclear reactors [2]. A typical advantage of selective laser sintering includes rapid prototyping and manufacturing objects of complex geometries. *SiC* materials, such as monoliths and composites, are promising materials for nuclear fuel cladding for LWRs and advanced reactors, components of fuel particles and pellets for reactor core structural components in fission reactors, including functional structures for fusion reactors [3]. Those applications depend on the central properties of *SiC*, such as excellent strength at higher temperatures, chemical inertness, comparatively low neutron absorption, and its stability to neutron irradiation up to high doses. The ability of *SiC* resistance to high-temperature as well as high-radiation environment proves *SiC* a candidate material for cladding fuels in light water reactors [4]. *SiC* remains intact even at temperatures beyond 1500 ^{0}C [5] and also parasitically captures fewer neutrons when compared to zircaloy, as well as possessing very low activation [6].

Protective coating on zirconium alloys has been a second choice proposed approach to enhancing Accident Tolerant Fuel (ATF) cladding concept [7]. The aim of this study is to investigate sintered *SiC* on *Zr-1Nb* alloy substrate under high temperature oxidation in air atmosphere in order to compare the oxidation behavior of sintering performed in air and argon SLS chamber.

2. Research methods

Zr-1Nb (E110) substrates of dimensions (20mm x 10mm x 2mm) were polished and wiped with an acetone filled cloth. An SLS system (IPG Photonics, Moscow, Russia) equipped with *Yb* fiber of output wavelength and maximum laser power of 1070 nm and 500 W respectively was used. This was then followed by sintering *SiC* (SIKA DENSITEC L) micro composite with minor phases including *Al2O3* and *Y2O3* onto the *Zr-1Nb* alloy. The figure 1 and table 1 represent the SLS system used and parameters followed in the deposition process respectively. The sample *b*, and ***c*** involve sintering of SiC on both sides of the substrates in air chamber while sample *d* and *e* were sintered in *Ar* filled chamber. After sintering, sample *a*, *b* and *d* were prepared for HT-Ox test by drilling through for flexible fixing into the furnace. The furnace was heated to the temperature of 1200 ^{0}C, which was accompanied by placing the samples into the heated furnace for 600 s, and quenched after in air. X-Ray Diffraction (XRD) phase composition was investigated with XRD 7000 diffractometer maxima (Shimadzu, Kyoto, Japan) along with the Sleve+ program. Qualitative and quantitative analyses were done with the Crystallographica Search-Match and PowderCell24 together with PDF-4+ database respectively. In addition, micro-indentation involving the Vickers hardness indenter was used with loads of 10N, 20N, 30N, 50N and 100N, which was accompanied by computing the depth of indenter penetration into the coating.

Table 1. SLS coating parameters

Samples	Laser power (W)	Scanning time (µs)	Laser speed (mm/s)	Coating thickness (µm)	SLS Chamber Atmosphere
b, c / d, e	125	500	25	200	Air/Ar

3. Results

Table 2 and figure 1 represent the results obtained after High Temperature Oxidation (HT-Ox) tests and the macrographs of the individual samples before and after the HT-Ox tests respectively. Observation of samples after HT-Ox shows a good dimensional stability of coated samples in *Ar* filled atmosphere than samples coated in air-filled atmosphere. The table 2 presents details of all samples, mass gain and percentage change ($P\Delta m$) in mass after HT-Ox tests. Sample *d* and *e*, which were coated in *Ar* atmosphere, recorded excellent dimensional stability, lowest mass gain (22.75 mg/cm2) as well as least increase in actual size (4.97 %) after HT-Ox. E110 alloy gave the highest mass gain as well as percentage increase of 34.62 mg/cm2 and 7.17 % respectively after HT-Ox test.

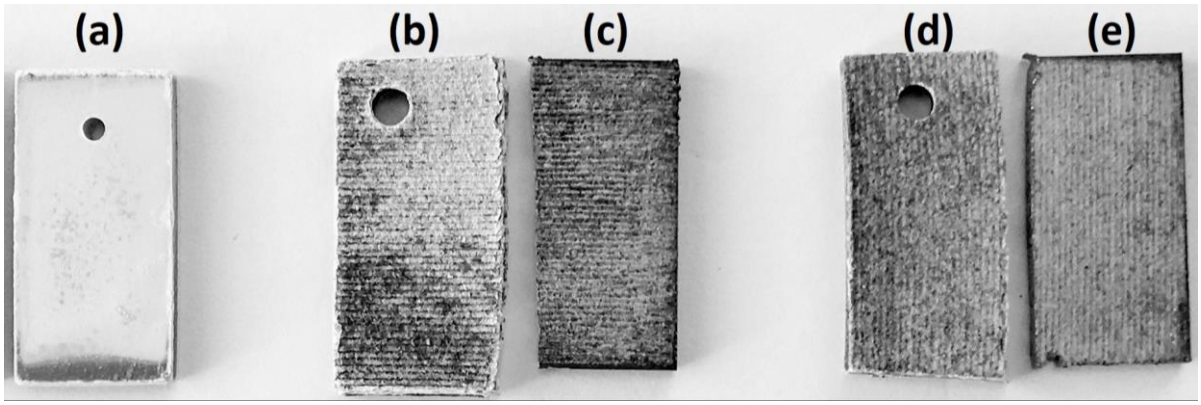

Figure 1. Macrograph of samples; (a) Zr-1Nb substrate, (b) SiC – Zr-1Nb [air] and (d) SiC – Zr-1Nb [argon] oxidized at 1200 ^{0}C for 600 s, Un-oxidized samples (c and e)

Table 2. Results of samples on mass-gain after HT-Ox test results

	Mass distribution

Samples	Description	Sintering atmosphere	HT-Ox	Before (g)	After HT-Ox (g)	Δm (g)	Mass gain (mg/cm2)	PΔm, %
a	E110 alloy	-	oxidized	2.511	2.691	0.180	34.62	7.17
b	SiC coated E110 alloy substrate	Air	oxidized	2.471	2.641	0.170	31.19	6.87
c		Air	-	-	-	-	-	-
d		Argon	oxidized	2.489	2.613	0.124	22.75	4.97
e		Argon	-	-	-	-	-	-

Figure 2 shows the main phases observed on surfaces of samples using the X-Ray Diffraction techniques. The uncoated E110 surfaces exhibited phase transformation from *Zr* hexagonal crystal structure to *ZrO2* monoclinic white crystalline structure of about 98.7 % and *Zr* hexagonal structure of 1.6 % after HT-Ox as shown in the table 3. This massive quantity of *ZrO2* phase formed after HT-Ox also accounted for the increase in the hardness about 4 times that of the bare E110 alloy which is evidenced on the figure 4. The table 3 shows the various phase transformation before and after HT-Ox. *SiC* coatings deposited in air and *Ar* atmosphere got transformed from *SiC, Al2O3*, and *Y2O3* to *SiC, SiO2* and *YAlO3* as shown in the table 3.

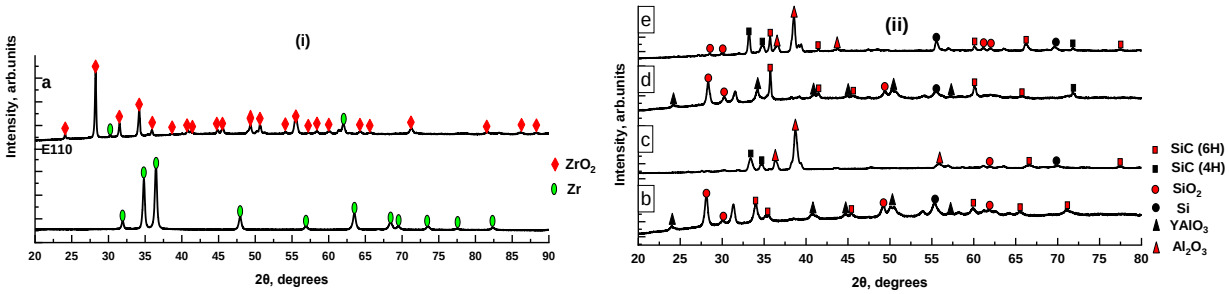

Figure 2. XRD phase composition of samples: (i) Oxidized E110-alloy (sample a) (ii) Sample *b, c, d, & e* as described and indicated in Table 2 and Fig 1 respectively

Table 3. Phase composition before and after HT-Ox test

Samples	Before HT-Ox	After HT-Ox
E110 alloy *(a)*	$Zr_{\text{hexagonal}}$	$ZrO2_{\text{monoclinic}}$ (98.7%), Zr_(1.3%)
Sintered in air *(c, b)*	$SiC_{\text{hexagonal}}$ (99.2%) $Al_2O_{3\ \text{tetragonal}}$ (0.8%) $Y_2O_{3\ \text{monoclinic}}$ (0.3%)	$SiC_{\text{hexagonal}}$ (44.5%) $SiO_{2\ \text{tetragonal}}$ (39.1%) $YAlO_{3\ \text{orthorhombic}}$ (16.4%)
Sintered in Ar *(e, d)*	$SiC_{\text{hexagonal}}$ (96.4%) $Al_2O_{3\ \text{tetragonal}}$ (3.2%) $Y_2O_{3\ \text{monoclinic}}$ (0.4%)	$SiC_{\text{hexagonal}}$ (49.4%) $SiO_{2\ \text{tetragonal}}$ (19.4%) $YAlO_{3\ \text{orthorhombic}}$ (34.2%)

Figure 3 shows the depth of penetration of the Vickers indenter into each sample as a function of the load applied. According to figure 3, all samples penetration depth increases as the indenter load increases. Moreover, there is a vast increase in the depth formed in bare E110 alloy, followed by high temperature oxidized E110 alloy (a) as compared to those of the coatings. For instance, at 100 N indenter load, the depth of indenter penetration and hardness for bare E110 alloy was about 56 microns and 238HV responsively, while after HT-Ox, depth of indenter penetration as well as the hardness measured was about 27 microns and 1023HV correspondingly resulting to about 4.3 times

the hardness and less than half the depth created in the bare E110 alloy. SiC coating sample in air atmosphere recorded the least indentation depth, followed by *Ar* atmosphere coated samples, and high temperature oxidized E110 alloy whiles bare E110 alloy being the most deeply indented.

SiC coatings prove to resist the indenter from creating unnecessary depth into samples due to the presence of oxides such as SiO2 and YAlO3 providing more than 50% covering of the samples surfaces after HT-Ox. Figure 4 also presents indentation elastic modulus as a function of the indenters' load. According to figure 4, it is very clear that bare E110 alloy indentation elastic modulus ranges uniformly between 207HV to 238HV followed by that of HT-Ox E110 alloy, which ranges between 782HV to 1101HV. Meanwhile, *SiC* coated samples recorded extremely higher hardness and indentation elastic modulus as evidenced in the figure 4 but also varies greatly from chosen areas on samples. This vast variation is due to the specific details of the area chosen for the indentation test and these includes the materials present at the area chosen, sintering track or in between track created during laser sintering. For instance, indentation performed on the sintered tracks will yield greater hardness as well as indentation elastic modulus than indentation tests performed along the track gaps which was later filled with the SiC powder. Therefore, sintering tracks needed to be closer to each other in order to minimize porous gaps on the surfaces of the coating. These gaps will also require a post finishing technique such as infiltrating the pores with pure Si and Cr using chemical vapor infiltration technique, which can be accompanied by polishing to closely eliminate pores on the sample's surfaces.

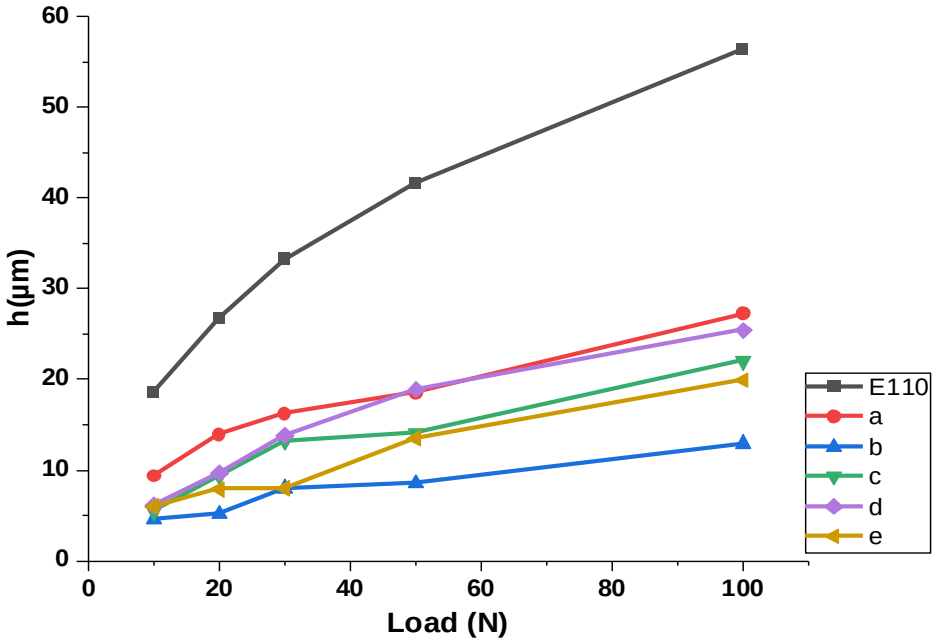

Figure 3. Graph of Indenter Load against depth of penetration in samples

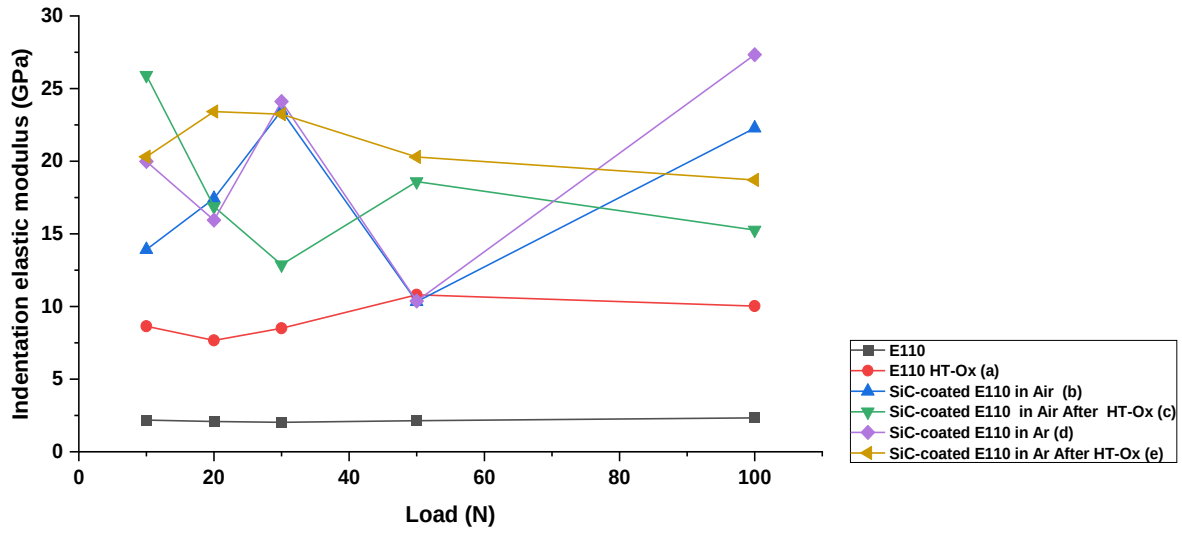

Figure 4. Graph of Indenter Load against Indentation Elastic Modulus of samples

4. Conclusion

SiC micro-composites were deposited on *E110* alloy substrates in air and *Ar* atmosphere and investigated under a high temperature oxidation environment in air at 1200 ^{0}C for 10 minutes towards fuel cladding material studies. Experimental measurement of mass gain, XRD phase content investigation and micro-indentation were conducted to study the behavior of the coating performed under air and argon atmosphere. The calculated mass gained and percentage mass change (*PΔm)* after the HT-Ox test was calculated to be 34.62 mg/cm2 (7.17%), 31.19 mg/cm2 (6.87%) and 22.75 mg/cm2 (4.97%) for bare *E110* alloy, *SiC-E110* sintered in air and argon SLS chamber respectively. XRD phase qualitative analysis reveals the formation of *ZrO2* above 90 % of the surface to sub-surface of the *E110* alloy after HT-Ox hence quadrupling the hardness of the initial *E110* alloy. In addition, *SiO2* and *YAlO3* became the main oxides yielding above 50 % and the remaining being *SiC* phases on the surface to sub-surface after HT-Ox test in coated samples. SiC coated samples in air and *Ar* yielded the least indentation depth as well as greater hardness before and after HT-Ox. Post finishing techniques involving chemical vapor infiltration is required to infiltrate the pores with pure Si or Cr in order to strengthen and eliminate porosity on the coated surfaces as well as polishing to ensure surface uniformity. The low outcomes of mass gained coupled with little changes in the dimensions of the *SiC* sintered sample fabricated in the *SLS* inert environment after HT-Ox proves optimistic and hence recommended for further research.

Acknowledgement.
The reported study was supported by the Russian Science Foundation (grant No. 19-19-00192).

References

[1] Attaran M 2017 The rise of 3-D printing: The advantages of additive manufacturing over traditional manufacturing. *Business Horizons* **60**(5) 677-688
[2] Terrani K, Jolly B & Trammell M 2020 3D printing of high-purity silicon carbide. *Journal of the American Ceramic Society* **103**(3) 1575-81
[3] Huang Y, Tillack M S & Ghoniem N M 2018 Tungsten monoblock concepts for the Fusion Nuclear Science Facility (FNSF) first wall and divertor. *Fusion Engineering and Design* **135** 346-355
[4] Ahn K 2006 Comparison of silicon carbide and zircaloy4 cladding during LBLOCA. *Massachusetts Institute of Technology Department of Nuclear Science and Engineering* **4**
[5] Younker I & Fratoni M 2016 Neutronic evaluation of coating and cladding materials for accident tolerant fuels. *Progress in Nuclear Energy* **88** 10-18

[6] Snead L, Nozawa T, Katoh Y, Byun T S, Kondo S & Petti D A 2007 Handbook of SiC properties for fuel performance modeling. *Journal of Nuclear Materials* **371**(1-3) 329-377
[7] Yang H Y, Zhang R Q, Peng X M and Wang M L 2017 Research progress regarding surface coating of zirconium alloy cladding. *Surf. Technol*. **46** 69–77